Rotation of Interchange Instability in the Large Helical Device

Yuki TAKEMURA, Satoru SAKAKIBARA[1], Kiyomasa WATANABE[1], Katsuji ICHIGUCHI[1],
Katsumi IDA[1], Yasuhiro SUZUKI[1], Satoshi OHDACHI[1], Yoshiro NARUSHIMA[1],
Ichihiro YAMADA[1], Kenji TANAKA[1], Hiroshi YAMADA[1] and LHD Experiment Group[1]

The Graduate University for Advanced Studies, Gifu 509-5292, Japan
[1]National Institute for Fusion Science, Gifu 509-5292, Japan

The rotation of resistive interchange instabilities excited in the periphery of plasmas compared to plasma flows under various plasma conditions in the Large Helical Device. The observed magnetohydrodynamic modes exhibit nominal rotation in the electron diamagnetic direction in the laboratory frame. We assumed that the ion (electron) flows consist of the $E \times B$ and ion (electron) diamagnetic drift flows. These drift flows were individually evaluated and geometrically compensated using a finite beta equilibrium. Experiments with different neutral beam injection conditions and different electron densities show that the frequencies of the observed modes were quantitatively consistent with those of the electron flow.

1. Introduction

Plasma rotation is a key parameter for not only the improvement of plasma confinement but also stabilization/destabilization of magnetohydrodynamic (MHD) instabilities. In tokamaks and reversed field pinches, tearing modes lead to major disruption after their rotation is stopped by the penetration of radial magnetic fluctuations to the vacuum wall [1]. In the classical tearing mode observed in ohmic plasmas, the rotation slows and is stopped when the electron density is lower than a threshold. It is also believed that the existence of an error field is one of the reasons for mode locking. An empirical scale has been constructed for estimating the tolerance of ITER and investigating the physical mechanism [2]. In high-beta plasmas, the resistive wall mode grows and terminates the plasma when the rotation is suppressed [3]. The mode can be stabilized by maintaining the rotation, which is realized by applying a toroidal momentum to the plasma externally [4].

The determinative factor of the mode frequency has been theoretically and experimentally investigated mainly in tokamaks. Because the rotation of the magnetic island produced by the tearing mode or others is a key parameter for stabilization effects due to an ion polarization current, the physical mechanism has been theoretically investigated using two fluid models [5].

Although mode rotation has been experimentally studied by comparing the plasma flows in several tokamaks [6, 7], it remains unclear. The rotation of the neoclassical tearing mode (NTM) was investigated recently in JT-60U [8]. According to that study, the mode frequency increased linearly with the toroidal ion flow driven by neutral

beam (NB) injection, whereas a gap appears between the mode rotation and toroidal flow. One possibility is that this is due to a poloidal flow such as a diamagnetic flow. Thus, a quantitative comparison of the observed frequency and plasma flow is required to understand the mode rotation mechanism.

An interchange mode, which is an important instability in helical plasmas, has long been experimentally and theoretically investigated to understand its characteristics and effect on plasma confinement [9]. However, experimental and theoretical knowledge of the rotation of the interchange mode is still insufficient. Experiments have shown that a large-amplitude mode causes significant minor collapse in the ideal unstable regime [10]. In particular, the $m/n = 1/1$ mode rotation started to slow when the plasma entered the ideal unstable regime because of an increase in the plasma current and the mode rapidly grew after the rotation stopped [11]. Here m and n are the poloidal and toroidal mode numbers, respectively. This is phenomenologically similar to the tearing locked mode, although the radial structure of the observed mode has a peak around the resonance, and the phase difference on the peak is almost the same, which suggests the characteristics of the interchange mode. Experimental study of the mode frequency in helical devices as well as tokamaks is important for future consider the stability control in the future.

This study describes the results of a comparison between the rotation of the interchange mode and plasma flow in the Large Helical Device (LHD) under various plasma conditions. Two types of experiments were performed to obtain different plasma flows. In one experiment, NBs were injected from different directions to

change the toroidal flow. In the other experiment, the electron density was scanned because the formation of the radial electric field depends on the electron density [12]. We focus on the mode excited in the periphery of the plasma because the peripheral modes are dominantly observed in a wide beta range, and they are key instabilities in the high-beta state in heliotron configurations [9]. Previous studies have identified them as resistive interchange modes [13]. In Sec. 2, the LHD and measurement systems are introduced, and the technique for geometrical compensation of the flow is provided in Sec. 3. Here we estimate the "global" plasma flow by compensating for the geometrical effects. The experimental results are given in Sec. 4. The discussion and summary are presented in the final section.

2. Experimental Setup

The LHD has a heliotron configuration with a pair of helical coils and three pairs of poloidal coils. The major and minor radii are 3.9 m and 0.65 m, respectively. The magnetic axis R_{ax} can be changed from 3.5 to 4.1 m. The available toroidal field at R_{ax}, B_{tax}, is less than 3 T. In the experiments described here, R_{ax} is set to 3.6 m and a plasma aspect ratio A_p of 6.3 was selected. In this configuration, the central and edge rotational transforms in vacuum are 0.5 and 1.5, respectively. In the experiments, the volume-averaged beta value evaluated by the diamagnetic flux measurements, $\langle \beta_{dia} \rangle$, was 1% - 1.5%. Although the rotational transform is spontaneously changed by finite beta effects, the profile is not significantly changed in this beta regime with a weak plasma current. The profile is predicted by the equilibrium mapping technique [14]. The LHD is equipped with three tangential and two perpendicular NBs. The tangential NBs were applied for production and maintenance of the plasma, whereas one perpendicular NB was used for measurement by charge exchange recombination spectroscopy (CXRS). Because two NBs are injected in the same direction and one is in opposite direction, we can change the dominant direction of the NBs by changing the polarity of B_{tax}. At negative B_{tax}, two co-NBs and a counter NB are available, and counterdominant operation is realized in the positive B_{tax} configuration. In experiments with different toroidal flows, both polarities of B_{tax} were applied to change the direction of the NBs, and a negative B_{tax} was set for the density scan experiments.

The magnetic fluctuations were measured with 21 magnetic probes, and the mode number was identified by a helical array with 15 probes and a toroidal array with 6 probes [15]. The radial profiles of the toroidal and poloidal carbon flows and ion temperature were measured by CXRS. The measured flows were used only for estimating the profiles of the radial electric field at a certain poloidal cross section through the momentum balance equation. The electric and magnetic fields at specific positions were estimated using the finite beta equilibrium estimated by the 3D MHD equilibrium code VMEC [16],

assuming a constant electric potential on each magnetic surface. The validity of this assumption was investigated in Ref. [17]. The electron temperature and density profiles were measured and the electron diamagnetic drift frequency was estimated using a Thomson scattering system. The techniques mentioned above are described in the next section.

3. Compensation of Geometrical Effects

Here a technique for estimating the $\boldsymbol{E} \times \boldsymbol{B}$ and electron (ion) diamagnetic flows at an arbitrary position is described. First, the profile of the radial electric field is estimated using the measured carbon flow and momentum balance equation,

$$E_r = \frac{1}{Z_c e n_c} \frac{dP_c}{dr} - (-v_{pc}B_t + v_{tc}B_p), \quad (1)$$

where E_r is the radial electric field on the midplane of the poloidal cross section where CXRS is applied, and Z_c and n_c are the number of charges and density of the carbon, respectively. P_c is the carbon pressure, and v_{pc} and v_{tc} are the poloidal and toroidal velocities of the carbon. B_t and B_p are the toroidal and poloidal magnetic fields at each measurement point. The first term of Eq. (1) is associated with the diamagnetic effect of the carbon and is neglected here. This is because the contribution from the first term is calculated to be only $\sim 10\%$ at the rational surfaces of the $m/n = 1/1$ and $3/4$ modes, assuming that the carbon density is the same as the charge exchange recombination emission intensity. The direction of E_r corresponds to that of the major radius R. Here we assume that the electric potential ϕ is constant on each magnetic surface. In the VMEC coordinates (s, φ, θ), the electric field can be expressed as

$$\boldsymbol{E} = -\nabla\phi = -\frac{d\phi}{ds}\nabla s, \quad (2)$$

where s is the normalized toroidal flux function, and θ and φ are the poloidal and toroidal components, respectively. Here $d\phi/ds$ can be estimated using E_r on the basis of finite beta equilibrium. The $\boldsymbol{E} \times \boldsymbol{B}$ drift velocity is defined as

$$\boldsymbol{v}_{E \times B} = \frac{\boldsymbol{E} \times \boldsymbol{B}}{B^2} = -\frac{d\phi}{ds}\nabla s \times \frac{\boldsymbol{B}}{B^2}. \quad (3)$$

Here we show $\boldsymbol{v}$ and $\boldsymbol{B}$ by using contravariant and covariant expressions. The contravariants of the poloidal velocity v^θ and toroidal velocity v^φ at the arbitrary point on a specific magnetic surface are as follows:

$$v^\theta = \frac{1}{B^2}\frac{1}{\sqrt{g}}\frac{d\phi}{ds}B_\phi, \quad (4)$$

$$v^\phi = -\frac{1}{B^2}\frac{1}{\sqrt{g}}\frac{d\phi}{ds}B_\theta, \quad (5)$$

where g is the Jacobian operator and can be obtained by VMEC solution. The covariant expressions of the velocities are

$$v_\theta = g_{\theta\theta}v^\theta + g_{\theta\phi}v^\phi, \tag{6}$$

$$v_\phi = g_{\theta\phi}v^\theta + g_{\phi\phi}v^\phi, \tag{7}$$

where

$$g_{\theta\theta} = \left(\frac{dX}{d\theta}\right)^2 + \left(\frac{dY}{d\theta}\right)^2 + \left(\frac{dZ}{d\theta}\right)^2, \tag{8}$$

$$g_{\theta\phi} = \frac{dX}{d\theta}\frac{dX}{d\phi} + \frac{dY}{d\theta}\frac{dY}{d\phi} + \frac{dZ}{d\theta}\frac{dZ}{d\phi}, \tag{9}$$

$$g_{\phi\phi} = \left(\frac{dX}{d\phi}\right)^2 + \left(\frac{dY}{d\phi}\right)^2 + \left(\frac{dZ}{d\phi}\right)^2. \tag{10}$$

Here $X = R\cos\varphi$ and $Y = R\sin\varphi$, and $v_{E\times B}$ is obtained as follows:

$$v_{E\times B} = \sqrt{v^\theta v_\theta + v^\phi v_\phi}. \tag{11}$$

The poloidal (toroidal) angular frequency of the $E \times B$ drift, $\omega_{\theta(\varphi)}$, can be evaluated through contour integration of $1/v_{E\times B}$ in the poloidal (toroidal) direction. Finally, the averaged $E \times B$ angular frequency, $\omega_{E\times B}$, is obtained by calculating $n\omega_\varphi - m\omega_\theta$.

The ion and electron diamagnetic drift velocities are defined as

$$v_i^* = \frac{1}{Z_i e n_i}\frac{dP_i}{ds}\nabla s \times \frac{B}{B^2}, \tag{12}$$

$$v_e^* = -\frac{1}{e n_e}\frac{dP_e}{ds}\nabla s \times \frac{B}{B^2}, \tag{13}$$

where P_i and P_e are the ion and electron pressures, respectively. We assumed that $Z_i = 1$ and $P_i = P_e$. The method of geometrical compensation is the same as that of $\omega_{E\times B}$. Finally, the averaged angular frequencies of ions and electrons, ω_i^* and ω_e^*, are obtained.

4. Experimental Results

4.1 Mode frequencies and plasma flows in typical low-beta discharge

Figure 1 shows the MHD activity in a typical discharge with $\langle\beta_{dia}\rangle \approx 1.5\%$. The two co-NBs and one counter NB were applied at 3.3 - 4.8 s to produce and maintain the plasma. In addition, two perpendicular NBs were alternately injected at 0.1 s intervals. One NB was used for the CXRS measurements and the other was applied to maintain a steady-state plasma. The port-through power of the NBs is about 20 MW. $\langle\beta_{dia}\rangle$ was almost constant during a discharge, while the line-averaged electron density was ramped up to 5×10^{19} m^{-3}. The $m/n = 3/4$ and 1/1 modes were dominantly observed and rotated in the electron diamagnetic direction in the laboratory frame. The $m/n = 3/4$ mode first appeared at the beginning of the discharge, and
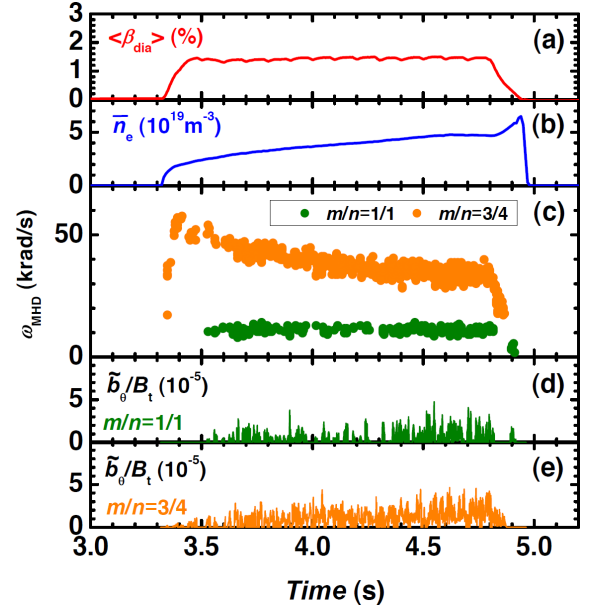

Fig. 1 MHD activity in discharge with $\langle\beta_{dia}\rangle \approx 1.5\%$. (a) Volume-averaged beta value, (b) line-averaged electron density, (c) angular frequencies of MHD modes, and amplitudes of the (d) $m/n = 1/1$ and (e) 3/4 modes.

the frequency increased with $\langle\beta_{dia}\rangle$. When $\langle\beta_{dia}\rangle$ exceeded about 1%, the frequency approached about 60 krad/s and then decreased with increasing density. The $m/n = 1/1$ mode appeared at 3.52 s when the density exceeded a certain value. The difference in the onsets of the modes can be interpreted as a difference in the pressure gradient on each rational surface. A gas puff was applied for fueling at the beginning of the discharge. Because the pressure typically increases from the plasma edge to core, the pressure gradient, which is the driving source of the interchange mode, also increases from the plasma edge [18]. Therefore, the mode located near the edge is destabilized earlier (as shown in Fig. 2). The frequency of the $m/n = 1/1$ mode was almost constant at about 10 krad/s. The amplitudes of the $m/n = 1/1$ and 3/4 modes, evaluated by the root mean square method, were 0.41 and 0.71, respectively, at 3.6 s, just after the excitation of the modes, and 0.77 and 1.30 at 4.7 s. They increased with the electron density even at constant $\langle\beta_{dia}\rangle$. Then, the electron temperature and magnetic Reynolds number S decreased by 71% and 41%, respectively. One of the reasons for the increasing amplitude is the reduction in S due to the decrease in the electron temperature. The reduction in S emphasizes the mode activity [13].

Figure 2 shows the profiles of the rotational transform, electron pressure, toroidal and poloidal velocities of the carbon, and radial electric field estimated according to Eq. (1). R_{ax} shifted from 3.6 m at the beginning of the discharge to 3.78 m at 3.76 s because of the increasing beta value. The resonant surfaces of the $m/n = 1/1$ and 3/4 modes are 4.41 m and 4.54 m, respectively, at 3.84 s.
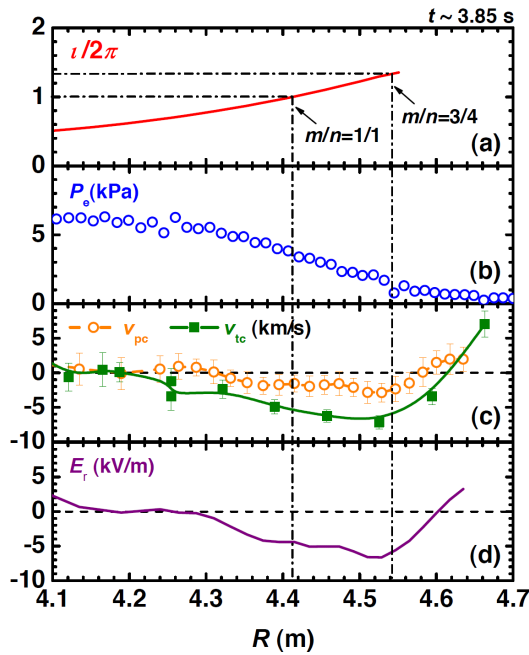
Fig. 2 Profiles of (a) rotational transform, (b) electron pressure, (c) toroidal and poloidal velocities of carbon, and (d) estimated radial electric field at 3.85 s in the discharge shown in Fig. 1.

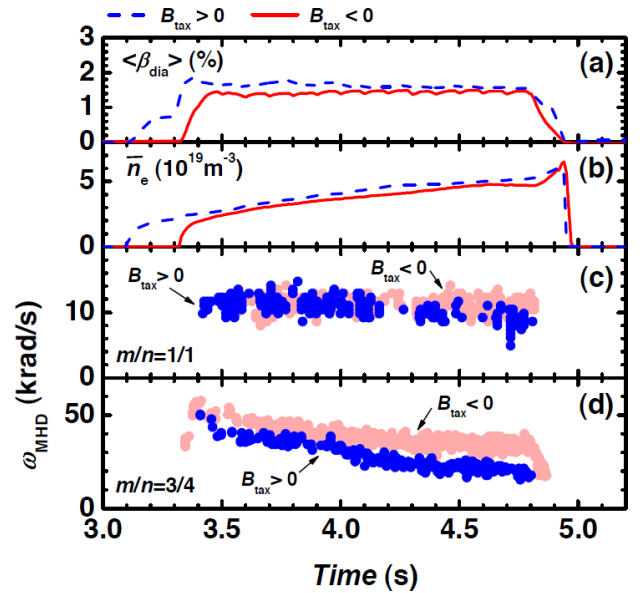

Fig. 3 Time evolution of (a) volume-averaged beta, (b) electron density, and angular frequencies of the (c) $m/n = 1/1$ and (d) 3/4 modes in negative and positive B_{tax} discharges.

The last closed flux surface (LCFS) is predicted to be located around 4.55 m, indicating that both modes were excited on the nested magnetic surfaces because the simulation result for a low beta equilibrium indicates that the magnetic surface inside the LCFS is nested [19]. The electron pressure has a smooth profile without any local flattening. The negative sign of the poloidal carbon velocity corresponds to the electron diamagnetic direction, whereas that of the toroidal velocity corresponds to the counter direction. The poloidal carbon flow was in the electron diamagnetic direction for R ranging from 4.31 to 4.58 m. The flow increased radially and approached about 3 km/s at $R = 4.53$ m. The toroidal flow is in the counter direction for R ranging from 4.19 to 4.62 m. The maximum was about 7 km/s at $R = 4.52$ m. Negative E_r formed at $R < 4.60$ m, and the maximum was about 7 kV/m at $R = 4.53$ m. The correlations between the MHD mode frequency and ion/electron flows are summarized in Sec. 4.3.

4.2 Relationship between MHD modes and plasma flows under different NB conditions

To investigate the effect of the toroidal flow on the MHD mode frequency, we changed the tangential NB direction by changing the polarity of B_{tax}. The positive and negative B_{tax} discharges are shown in Fig. 3. B_{tax} was set at -1.75 T for negative B_{tax} and 1.375 T for positive B_{tax}. $\langle \beta_{dia} \rangle$ was almost constant, and the line-averaged electron density increased during the discharge. Their val-

ues and temporal changes are similar in both cases. The achieved $\langle \beta_{dia} \rangle$ and line-averaged electron density at 3.85 s are 1.40% and 3.39×10^{19} m^{-3} in the $B_{tax} < 0$ discharge, whereas they are 1.65% and 3.76×10^{19} m^{-3}, respectively, in the $B_{tax} > 0$ one. The frequency of the $m/n = 1/1$ mode is about 10‑15 krad/s and is almost the same in both cases. For the $m/n = 3/4$ mode, the frequency is slightly different. In the negative B_{tax} case, the frequency is about 10 krad/s higher than that in the positive B_{tax} case.

Figure 4 compares the toroidal/poloidal flows and electron pressure in both cases. Although the direction of the poloidal flow is the electron diamagnetic one at both resonances, the direction of the toroidal flow is different. The toroidal flow in the negative (positive) B_{tax} case is in the counter (co-) direction. The absolute value of the toroidal flow approached the same level in both cases. The pressure gradient in the negative B_{tax} case is larger than that in the positive B_{tax} case at $R > 4.24$ m. The FIT3D code [20] predicts this and attributes it to the difference in the NB deposition profile because the port-through power for negative B_{tax} is 4.6 MW larger than that for positive B_{tax}.

The time evolution of the estimated $\omega_{E \times B}$ and ω_e^* for the $m/n = 3/4$ resonance are shown in Fig. 5. These frequencies were estimated using the technique described in Sec. 3. Here $\omega_{E \times B}$ is almost the same in both discharges despite the significant difference in the toroidal flow. This suggests that the difference has little effect on the formation of the radial electric field. However, ω_e^* differed significantly between the two discharges because of the difference in the pressure gradient. The difference in ω_e^* is about 10 krad/s and is the same as that in the angular fre-
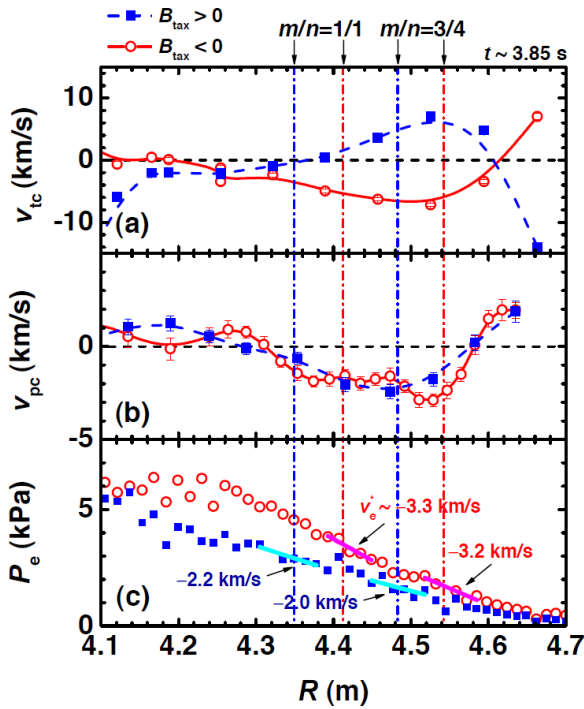
Fig. 4   Profiles of (a) toroidal and (b) poloidal flows, and (c) electron pressure at $t = 3.85\,\mathrm{s}$ in the negative and positive B_{tax} discharges shown in Fig. 3.

quency of the $m/n = 3/4$ mode. The angular frequency of the $m/n = 3/4$ mode and $\omega_{E\times B} + \omega_{\mathrm{e}}^*$ are compared in Fig. 6. The temporal change in the mode frequency and the absolute value are quantitatively consistent with those of the electron flow. The experimental results indicate that the toroidal ion flow itself does not directly affect the mode rotation but contributes to it through the formation of the radial electric field, at least in the present range of the toroidal flow.

4.3   Summary of comparison of plasma flow under various plasma conditions

Finally, the electron density was varied in the range 2.4×10^{19} to $4.8 \times 10^{19}\,\mathrm{m}^{-3}$ so as to change the radial electric field because the formation of the radial electric field is sensitive to the density according to Eq. (1). The mode frequencies also depend on the density, as shown in Fig. 1. $\langle \beta_{\mathrm{dia}} \rangle$ varied from 1.1% to 1.6%. Figure 7 compares the angular frequencies of the observed modes and the ion/electron flows in four discharges. The results shown in Fig. 6 are included here. Positive frequency corresponds to the electron diamagnetic direction. The $E \times B$ flows obtained in the experiments were in the electron diamagnetic direction, and the electron flow with $\omega_{E\times B} + \omega_{\mathrm{e}}^*$ could be widely varied. The experimental results show that the frequencies of the electron flows agree quantitatively with those of the $m/n = 1/1$ (at < 20 krad/s) and 3/4 (at > 20 krad/s) modes. Although the charge number
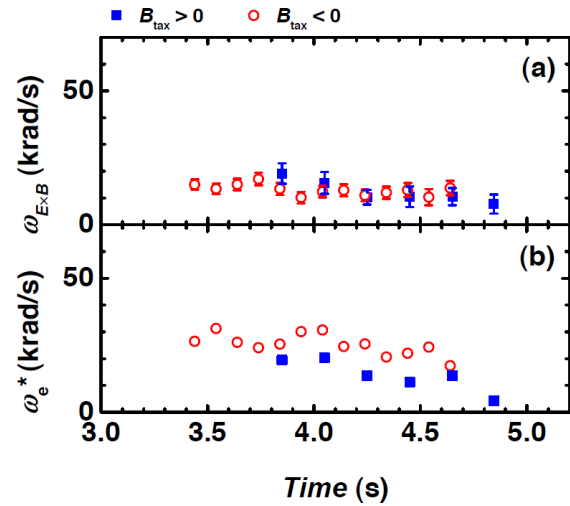

Fig. 5   Time evolution of angular frequencies of (a) $E \times B$ drift and (b) electron diamagnetic drift in the negative (closed squares) and positive (open circles) B_{tax} discharges.
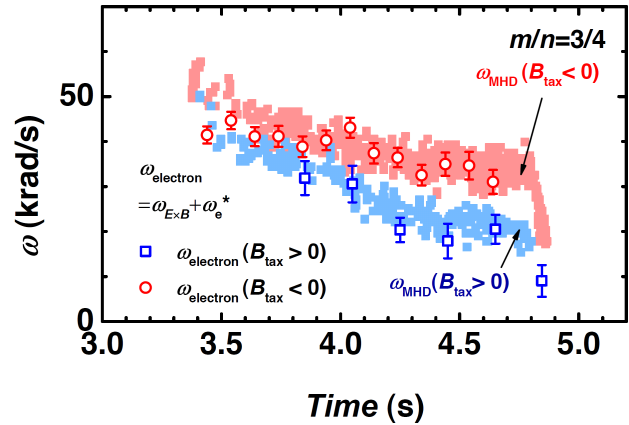

Fig. 6   Relationship between angular frequency of the $m/n = 3/4$ mode (closed circles and squares) and sum of angular frequencies of $E \times B$ and electron diamagnetic flows (open circles and squares).

is assumed to be unity in the estimation of ω_{i}^*, the result is insensitive to this because the modes rotate in the electron diamagnetic direction with higher frequency than the $E \times B$ flows.

5.   Discussion and Summary

The rotations of resistive interchange modes excited in the periphery were compared to the ion and electron flows, defined as each diamagnetic drift flow and the $E \times B$ drift flow. The experiments with different types of NB injection and different electron densities indicate that the observed modes with $m/n = 1/1$ and 3/4 are clearly dragged by the electron flow. The difference in the $m/n = 3/4$ mode frequencies in both discharges, as shown in Fig. 3 (d), is caused by the difference in ω_{e}^* because of the pressure gra-
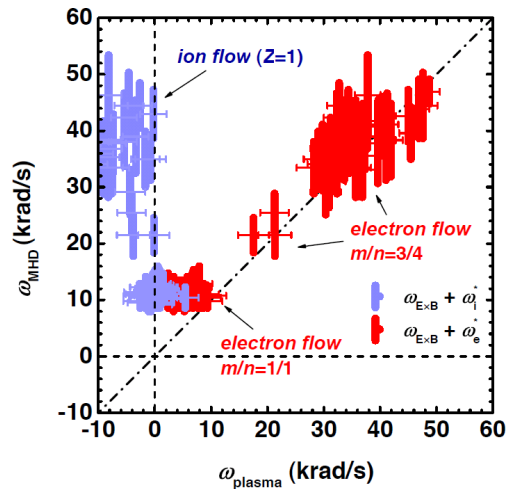
Fig. 7 Comparison of angular frequencies of the $m/n = 1/1$ and 3/4 modes and the electron/ion flows obtained in plasmas with different electron densities.

dient. Thus, the reason for the slowing of the mode rotations is the reduction in ω_e^* due to an increase in the electron density.

The rotations of the $m/n = 1/1$ and 3/4 modes appear to depend very little on the toroidal ion flow when it is less than 7 km/s. The rotation of the $m/n = 2/1$ NTM observed in tokamak devices was dragged mainly by the toroidal ion flow [8], which is concluded on the basis of a comparison with the case for ion velocities of up to 100 km/s. In addition, there is a gap between the angular frequencies of the NTM and toroidal ion flow, which might be due to the poloidal flow. Thus, experiments in a wider range of toroidal flows are required to clarify the direct effect on the mode rotation.

When the interchange mode grows significantly in the ideal unstable regime, minor collapse was found to occur after the $m/n = 1/1$ mode rotation slowed and stopped [12]. The mode rotated in the electron diamagnetic direction at the beginning of the discharge, and the rotation started to slow when the amplitude exceeded a threshold. Although no plasma flow was measured then, it is expected that the deceleration of the mode rotation is caused by a reduction in the electron diamagnetic drift flow due to the flattening of the pressure profile around the resonance and/or by deceleration of the electron flow velocity due to the formation of a magnetic island. The experiments described in this study were done in the ideal stable regime. The amplitudes of the observed modes were sufficiently small compared with those of the ideal unstable case. No profile flattening was observed in any discharge.

In summary, the rotation of resistive interchange instabilities was compared to plasma flows under various plasma conditions in the LHD to investigate the physical mechanism of the rotation. The observed MHD modes typically rotate in the electron direction in the laboratory frame, assuming that the ion (electron) flows consist of the $\boldsymbol{E} \times \boldsymbol{B}$ drift and ion (electron) diamagnetic drift flows, and their flows were geometrically compensated using a finite beta equilibrium. To change the radial electric field and toroidal flow velocity, the electron density was scanned and the direction of the NBs was changed. The experimental results show that the frequency of the observed mode is quantitatively consistent with the sum of $\boldsymbol{E} \times \boldsymbol{B}$ and the electron diamagnetic flows, which suggests that the rotation of the resistive interchange mode is dragged by the electron flow.

Acknowledgments

[1] M.F.F. Nave and J.A. Wesson, Nucl. Fusion **30**, 2575 (1990).
[2] J.E. Menard *et al.*, Nucl. Fusion **50**, 045008 (2010).
[3] E.J. Strait *et al.*, Phys. Rev. Lett. **74**, 2483 (1995).
[4] S. Takeji *et al.*, Nucl. Fusion **42**, 5 (2002).
[5] R. Fitzpatrick, P.G. Watson and F.L. Waelbroeck, Phys. Plasmas **12**, 082510 (2005).
[6] J. Schirmer *et al.*, Proc. 34th EPS Conference on Plasma Phys. Warsaw, 2 - 6 July 2007 ECA Vol.31F, P-1.133 (2007).
[7] J.A. Snipes *et al.*, Nucl. Fusion **30**, 205 (1990).
[8] A. Isayama *et al.*, Plasma Fusion Res. **5**, 037 (2010).
[9] S. Sakakibara *et al.*, Fusion Sci. Technol. **58**, 176 (2010).
[10] S. Sakakibara *et al.*, Fusion Sci. Technol. **50**, 177 (2006).
[11] Y. Takemura *et al.*, Nucl. Fusion **52**, 102001 (2012).
[12] K. Ida *et al.*, Nucl. Fusion **45**, 391 (2005).
[13] S. Sakakibara *et al.*, Plasma Phys. Control. Fusion **50**, 124014 (2008).
[14] C. Suzuki *et al.*, Plasma Phys. Control. Fusion **55**, 014016 (2012).
[15] S. Sakakibara, H. Yamada and LHD Experiment Group, Fusion Sci. Technol. **58**, 471 (2010).
[16] S.P. Hirschman, W.I. van Rij and P. Merkel, Comput. Phys. Comm. **39**, 143 (1986).
[17] S. Nishimura *et al.*, Phys. Plasmas **7**, 437 (2000).
[18] S. Sakakibara *et al.*, Nucl. Fusion **41**, 1177 (2001).
[19] Y. Suzuki *et al.*, Proc. of Joint Conf. 17th Int. Toki Conf. 16th Int. Stellarator/Heliotron Workshop 2007, Oct. 15-19, 2007, Toki, CD-ROM Pa2-043 (2007).
[20] S. Murakami *et al.*, Trans. Fusion Technol. **27**, 256 (1995).